Heliyon 10 (2024) e31970

Contents lists available at ScienceDirect

Heliyon

journal homepage: www.cell.com/heliyon

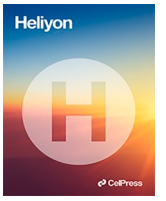

Research article

Stem cell index-based RiskScore model for predicting prognosis in thyroid cancer and experimental verification

Ruoran Chen, Wei Gao *, Linlang Liang, Hao Yu, Wei Song

Department of Endocrinology, General Hospital of Northern Theater Command, Shenyang, 110016, China

A R T I C L E I N F O

Keywords:
Thyroid cancer
Stem cell
mRNAsi
Molecular subtypes
Prognostic model
Immunotherapy

A B S T R A C T

Objective: An mRNA expression-based stemness index (mRNAsi) has been developed to characterize cancer stemness. However, the predictive value of mRNAsi-based signature in therapeutic resistance and immunotherapy in thyroid cancer (THCA) remains unclarified. This study evaluated and validated the role of mRNAsi in drug sensitivity, its relationship between mRNAsi and THCA clinical features and immunity based on bioinformatics.

Methods: Based on transcriptome data of THCA patients from the Tumor Genome Atlas Project (TCGA) database, and expression data of multifunctional stem cell samples from the Progenitor Cell Biology Consortium (PCBC) databases, mRNAsi was calculated by the " one class logistic regression (OCLR)" method, Molecular subtypes of TCGA-THCA samples were identified with mRNAsi-related genes using ConsensusClusterPlus method. The gene mutation, clinical characteristics, immune characteristics, TIDE and drug sensitivity were compared among molecular subtypes. A prognostic model was designed with Lasso cox method. Modulation of malignant phenotype of THCA cell lines by model characterization genes is validated by CCK-8, flow cytometry. DNA methylation disorder in promoter region was analyzed between risk groups. The model was validated for survival in the internal Test dataset, while TCGA pan-cancer and immunotherapy datasets were further employed to validate the performance of this model.

Results: We obtained a total of 78 stem cell samples, each containing the expression profile of 8087 mRNA genes. Based on mRNAsi, THCA was divided into 3 subtypes. Subtype C2 had the poorest prognosis and highest immune score, while subtype C3 had the best prognosis, lowest mRANsi and highest TIDE score. Patients in subtype C2 showed higher sensitivity to Cisplatin, Erlotinib, Paclitaxel, and Lapatinib. The prognostic signature was generated using 5 mRNAsi-related genes, which could predict prognosis for THCA. qRT-PCR results showed that the expression of 5 genes were various in Hth7 and KTC-1 cells, and inhibition CELSR3 expression increased percentage of apoptosis in Hth7 and KTC-1 cells. mRNAsi related DNA methylation sites were mainly enriched in tumor related pathways. Good performance of this model was validated in Test dataset, pan-cancer and immunotherapy datasets.

Conclusion: This study identified three subtypes for classification and developed a prognostic model with mRNAsi-related genes, which provided great potential for prognosis and immunotherapy prediction.

* Corresponding author.
E-mail address: 13555785785@163.com (W. Gao).

https://doi.org/10.1016/j.heliyon.2024.e31970
Received 4 February 2024; Received in revised form 22 May 2024; Accepted 24 May 2024
Available online 25 May 2024

1. Background

Thyroid cancer (THCA) makes up about 94.5 % of all endocrine tumors, establishing itself as the most prevalent endocrine cancer [1]. The gender, race, and region are factors associated with the incidence of THCA. When comparing the genders, women have a incidence rate three times higher than men. The incidence of THCA has been increasing rapidly in recent years, with an annual rise of nearly 4 %. Papillary thyroid carcinoma (PTC) accounts for around 80 % of THCA cases, making it the most common form of the disease. The majority of patients with PTC experience slow progression and have a favorable prognosis. However, patients with vascular invasion, extra-thyroidal invasion, or distant metastasis often face a poor prognosis [2,3]. Standard treatment (surgery or radioactive iodine therapy) is effective for most patients [4], but there are still some patients who are not sensitive to available treatments [5]. Therefore, a deeper knowledge on THCA pathogenesis is essential to explore new therapeutic measures and to improve its prognosis.

The development of THCA is a multistep, cascade process involving genetic mutations, immune cell and dysfunction, disrupted hormone levels, and cancer stem cells (CSC) [6–8]. In 1997, Bonnet et al. provided the first conclusive evidence of CSC in leukemia patients, opening up new perspectives in human understanding of tumors [9]. It has been documented that CSC has the property of self-renewal and differentiation that is involved in tumor development, metastasis, heterogeneity, recurrence, and drug resistance [10–12]. Targeting CSC-associated surface biomarkers, pathways or CSC microenvironment have showed a potential for cancer therapy [13,14]. Pan, X et al. revealed that CSC marker genes BIRC5, PTTG1, CENPF and CDKN3 were correlated with unfavorable prognosis of collecting duct renal cell carcinoma [15]. A CSC marker, PAF1 was reported to down-regulate markers of self-renewal and maintenance of CSCs as well as metastasis-relevant gene markers [16]. What's more, targeting CSC marker gene SMOC-2 was found to improve chemotherapy tolerance and suppress cell proliferation in endometrial carcinoma [17]. Currently, previous theories suggest that THCA originates from stem cells, progenitor cells, or dedifferentiated mature thyroid cells, but because somatic cells are short-lived, CSC or progenitor cells are the most likely source of THCA [18]. Available evidence suggests that THCA is composed of heterogeneous cells, of which only subpopulations with stem cell-like characteristics are tumorigenic [19]. Moreover, the differentiation pathway of thyroid CSC is abnormal and the developmental process is blocked due to the lack of specific markers that control the degree of differentiation. If the blockage occurs late in the differentiation process, it leads to highly differentiated THCA, and if it occurs early, it produces hypodifferentiated THCA [20]. The above evidence fully illustrates the importance of CSC in THCA onset and differentiation.

Since the diagnosis and treatment of THCA is closely related to its pathogenesis and about 1/3 of thyroid malignancies may be underdiagnosed, which brings difficulties to clinical diagnosis and treatment [21]. Therefore, the search for THCA diagnostic and early warning molecules is an important part of THCA clinical research. We therefore explored the diagnosis of THCA based on TCGA and PCBC databases, explored the expression of mRNAsi indicators reflecting the gene expression characteristics of stem cells in THCA, studied the correlation between clinical characteristics and mRNAsi and immunity of THCA, assessed the role of mRNAsi in drug sensitivity, and performed validation. A significant correlation was found between mRNAsi as a potential biomarker and the clinical features of THCA, and its great potential for the therapeutic and prognostic determination of THCA.

2. Methods

2.1. Data sources and processing

Clinical and mRNA transcriptome data of THCA patients were obtained from TCGA GDC (https://portal.gdc.cancer.gov/), and expression data of multifunctional stem cell samples were obtained from PCBC database (https://progenitorcells.org/frontpage). We performed the following preprocessing on the downloaded TCGA-THCA data: (1) keep the samples with gene expression profile information and convert Ensembl ID to Gene Symbol; (2) remove the samples lacking survival information; (3) take the median value when the same gene has multiple gene expression cases; (4) convert RNA seq expression to TPM value and perform log2 conversion. The methylation dataset of Illumina HumanMetallation 450 BeadChip of thyroid cancer patients was obtained from the TCGA database, from which the methylation sites in the promoter region of key genes were extracted.

2.2. Stem cell index calculation based on OCLR method

We employed OCLR technique to predict and compute the stem cell index [22]. First, only the sample data of embryonic stem cells (ESC and pluripotent stem cells (iPSC), collectively referred to as stem cell (SC) samples were retained. Gene expression data from selected stem cell samples were centered, i.e., their average expression values were subtracted from each gene expression value to eliminate bias between different samples. Then, the obtained gene expression profiles of genes encoding proteins were centralized using the mean values and finally the weight vector of each gene was calculated in the "gelnet" R package (https://cran.r-project.org/web/packages/gelnet/index.html).

In the TCGA-THCA cohort, we calculated Spearman's correlation coefficients between the expression profile of sample gene and the model gene weight vector. The Spearman correlation coefficients were then linearly transformed [23] by the following method :

$$\text{Stem cell index} = \frac{(\text{Spearman's correlation coefficient} - \text{Spearman's minimum correlation coefficient})}{\text{Spearman's maximum correlation coefficient}}$$

The mRNAsi values range from 0 to 1, where a value closer to 1 indicates cells that are less differentiated and possess more robust stem cell characteristics.

2.3. Correlation between stem cell index and THCA mutation, clinical, and immune characteristics

The TCGA-THCA cohort mutation dataset was downloaded by the MuTect2 module [24], followed by our screening of genes with mutation frequencies greater than or equal to 3 and comparing the differences between mRNAsi between THCA mutant type and wild-type samples.

Basic clinical information of THCA patients included M-stage, gender, age, N-stage, T-stage, and pathological stage. Next, mRNAsi expression differences between tumor samples with different clinical characteristics grouping were compared using unpaired *t*-test or Wilconxon *t*-test.

The link between thyroid cancer stem cell indices and immune and stromal scores was analyzed by determining the relative abundance of 22 immune cells and the percentage of immune cells using the "CIBERSORT" function in the "bseqsc" R package and the "ESTIMATE" algorithm in the "ESTIMATE" package, respectively. Single Sample Gene Set Enrichment Analysis (ssGSEA) was performed to score 28 types of immune cells, and then Pearson correlations between immunity, matrix scores, and mRNAsi were also computed [25–27]. TCGA-THCA and GSE3467 dataset were used to analyze mRNAsi and calculated the correlation between mRNAsi and immune scores. Additionally, we obtained a total of 162 cancer driver genes from the published research [28] and analyzed their correlation with mRNAsi.

2.4. Survival analysis of stem cell index

For survival analysis of cancer stem cell indexes, the optimal cutoff of mRNAsi was determined using surv_cutpoint in survminer package, and the survival differences between the two groups were compared by log-rank test.

2.5. Molecular subtyping based on mRNAsi-related genes

We calculated the correlation between protein coding gene (PCG) and mRNAsi in TCGA dataset, and obtained the genes associated with mRNAsi by filtering with the threshold $|R| > 0.4$ and $P < 0.05$. Using ConsensusClusterPlus R package, the samples in the TCGA-THCA cohort were then clustered by the "K-M" algorithm and "1-Pearson correlation" as the metric distance [29]. Following 500 bootstraps, where each bootstrap ran 80 % of the patients from the training set and 20 % of the patients from the validation set, the ideal number of clusters was established using the cumulative distribution function (CDF). The classification of molecular subtypes was the most accurate according to the consistency matrix and consistency cumulative distribution [30].

2.6. TIDE of different subtypes and drug sensitivity study

One of the accepted therapies for THCA has gradually evolved into immune checkpoint inhibitor-based therapy [31]. Potential clinical effects of immunotherapy on the current molecular subtypes were assessed using the TIDE (http://tide.dfci.harvard.edu/) software to determine the differences in immunotherapy responsiveness between molecular subtypes, with a higher TIDE score suggesting less immunotherapy benefits and greater possibilities of immune escape [32]. Lastly, drug sensitivity to THCA was predicted with the "pRRophetic" package [33].

2.7. Development of a prognostic model and verification

For genes related to mRNAsi, we randomly grouped the data in the TCGA dataset in a ratio of Train: Test = 1:1. Then, we conducted a univariate COX analysis in the Train grouping dataset to screen for prognostic related genes. Next, lasso cox regression analysis was carried out via R software package glmnet [34], following by performing stepwise regression and the Akaike information criterion (AIC). Finally, each sample was calculated for a prognostic RiskScore with the selected genes and further normalized with the formula defined as below:

RiskScore = coefficient1*gene1 expression + … + coefficientN*geneN expression.

The RiskScore of each sample was calculated with above formula and normalized with Zscore. Patients showing a Zscore >0 were classified into high-risk groups, otherwise they were classified into low-risk groups. Two-group survival differences were compared with log-rank test.

2.8. Differential analysis of DNA methylation profile of risk genes and screening of mRNAsi related epigenetic regulatory pathways

The correlation between these sites and gene expression was calculated, and the differences of these methylation sites between high- and low risk were further analyzed applying champ. DMP function embedded in "ChAMP" package in R [35]. In addition, we also executed the functional enrichment analysis to reveal the regulatory role of differential methylation genes between RiskScore groups [36].

2.9. Cell culture and transient transfection

DMEM F12 supplemented with 10 % FBS (Gibco, Thermo Fisher, USA) was used to culture three types of human thyroid cancer cell Lines (Hth7, KTC-1 and Human normal thyroid epithelial cells Nthy-ori3-1) obtained from Beijing National Cell Bank of China (BNCC, Beijing, China). The cells were grown at 37 °C with 5 % CO_2 in a humidified environment. The target sequences for CELSR3 siRNA were as follows:

Gene	target sequence (5′–3′)
si CELSR3#1	CACCTGATACTCCTTTTGTGATA
si CELSR3#2	ACCTGATACTCCTTTTGTGATAA

2.10. Quantitative reverse transcription-polymerase chain reaction (qRT-PCR)

Total RNA was extracted from Nthy-ori3-1, Hth7, and KTC-1 cell lines using TRIzol reagent from Thermo Fisher (U.S.A.). QRT-PCR was conducted with the use of FastStart Universal SYBR Green Master in a Roche (U.S.A.) LightCycler 480 PCR system to isolate RNA from each sample (2 μg). The reaction volume for qRT-PCR was 20 μl that consisted of 0.5 μl of forward and reverse primers, an appropriate amount of water, 2 μl of cDNA template, and 10 μl of PCR mixture. Briefly, the PCR reaction conditions were as follows: firstly, the strand was unstranded for 30 s at 95 °C and then 45 cycles were performed, each consisting of 15 s (s) at 94 °C, 30 s at 56 °C, and 20 s at 72 °C. Three independent analyses were run for each sample. Quantification was performed from threshold cycling (CT) data using the $2^{-\Delta\Delta CT}$ method and standardized to the level of GAPDH. The mRNA expression levels in both the normal tissues and control tissues were compared. The chart below listed primer pair sequences for the genes targeted:

Gene	Forward primer sequence (5′–3′)	Reverse primer sequence (5′–3′)
CELSR3	GGTGCTGAGATTGGCAACTACTC	CAGCCGATGAAGTCCTTATGGG
F3	CAGAGTTCACACCTTACCTGGAG	GTTGTTCCTTCTGACTAAAGTCCG
NTF3	CTACTACGGCAACAGAGACGCT	GGTGAGGTTCTATTGGCTACCAC
STARD9	AGGTGGACAATCGACCAGATG	CCAGTAGCAGTAATCAAAGCCAA
TMEM130	GCTCCTATCTCACTAAGACCGTC	CACGGAGTCTTCAGTCACCATC
GAPDH	GTCTCCTCTGACTTCAACAGCG	ACCACCCTGTTGCTGTAGCCAA

2.11. Cell viability

Differently treated cells were cultured at a density of 1×10^3 cells/well in 96-well plates and added with CCK-8 solution (Beyotime, China) was applied at given time points. The O. D 450 value in each well was detected using a microplate reader (Thermo Fisher, USA).

2.12. Flow cytometry

The cells were harvested with trypsin and then resuspended at the concentration of 1×10^5/200 μL in PBS. Next, Annexin V-FITC and PI solution were applied for dyeing the cells for 30 min on ice in the dark. After PBS washing, a BD FACS Calibur flow cytometer (BD, USA) was used to detect the samples for analyzing cell apoptosis.

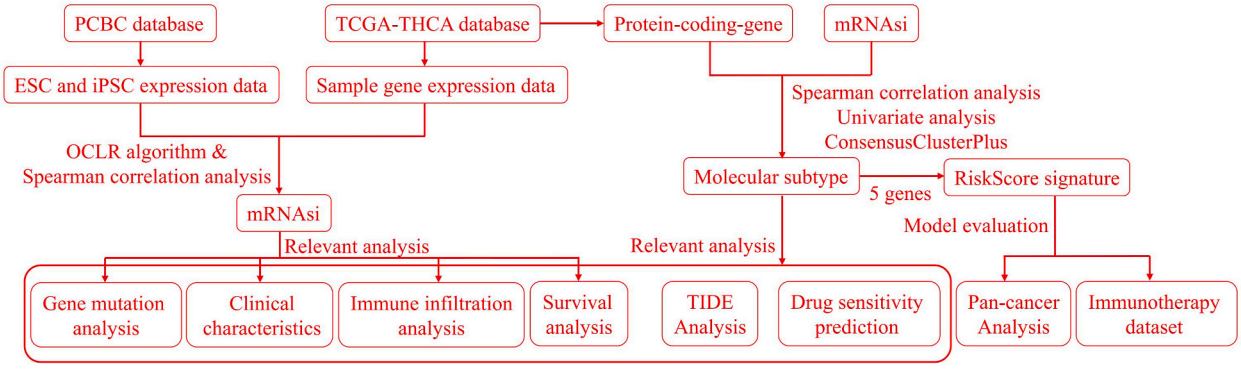

Fig. 1. The workflow chart for this study.

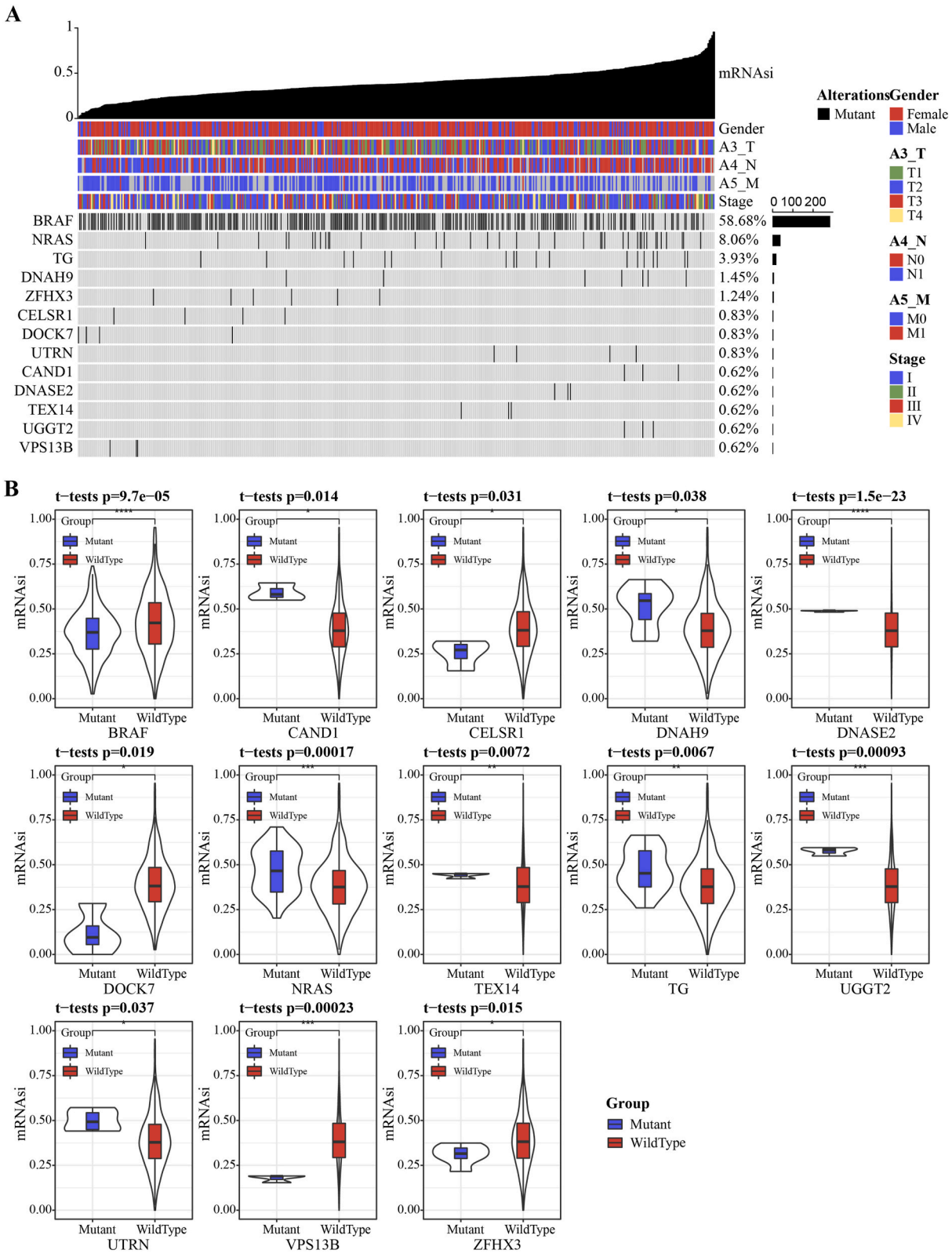

Fig. 2. Relationship between stem cell indices and molecular mutation subtypes. A: demonstration of mRNAsi index with clinical characteristics and mutation status; B: comparison of mRNAsi in mutant and non-mutant subgroups. *P < 0.05; **P < 0.01; ***P < 0.001; ****P < 0.0001. ns: not significant.

2.13. Statistical analysis

All statistical analyses were conducted in R software (version 4.1.3, https://www.r-project.org/) and all statistical tests were bilateral unless otherwise specified. The prognostic differences were described through Kaplan-Meier curves along with log-rank test. $P < 0.05$ was defined as statistically significant.

3. Results

3.1. Correlation between stem cell index and molecular mutation subtypes

The workflow of this research was exhibited in Fig. 1. According to the OCLR calculation method, we obtained a total of 78 SC samples from the PCBC database, each containing the expression profiles of 8087 mRNA genes. In addition, we downloaded the mutation dataset processed by Mutect2 software in TCGA database and screened 338 genes with mutation frequency ≥3 from the TCGA database. To better visualize the relationship between mRNAsi index and clinical features as well as molecular mutation subtypes in TCGA-THCA samples, we ranked THCA samples according to mRNAsi index from smallest to largest and then compared clinical data with mutations. BRAF, NRAS, and TG were found to be the top three most commonly mutated genes, with mutation frequencies of 58.68 %, 8.06 %, and 3.93 %, respectively (Fig. 2A). To compare whether the mRNAsi index differed among the different molecular mutation subtype samples, we compared the differences between mRNAsi between samples with and without

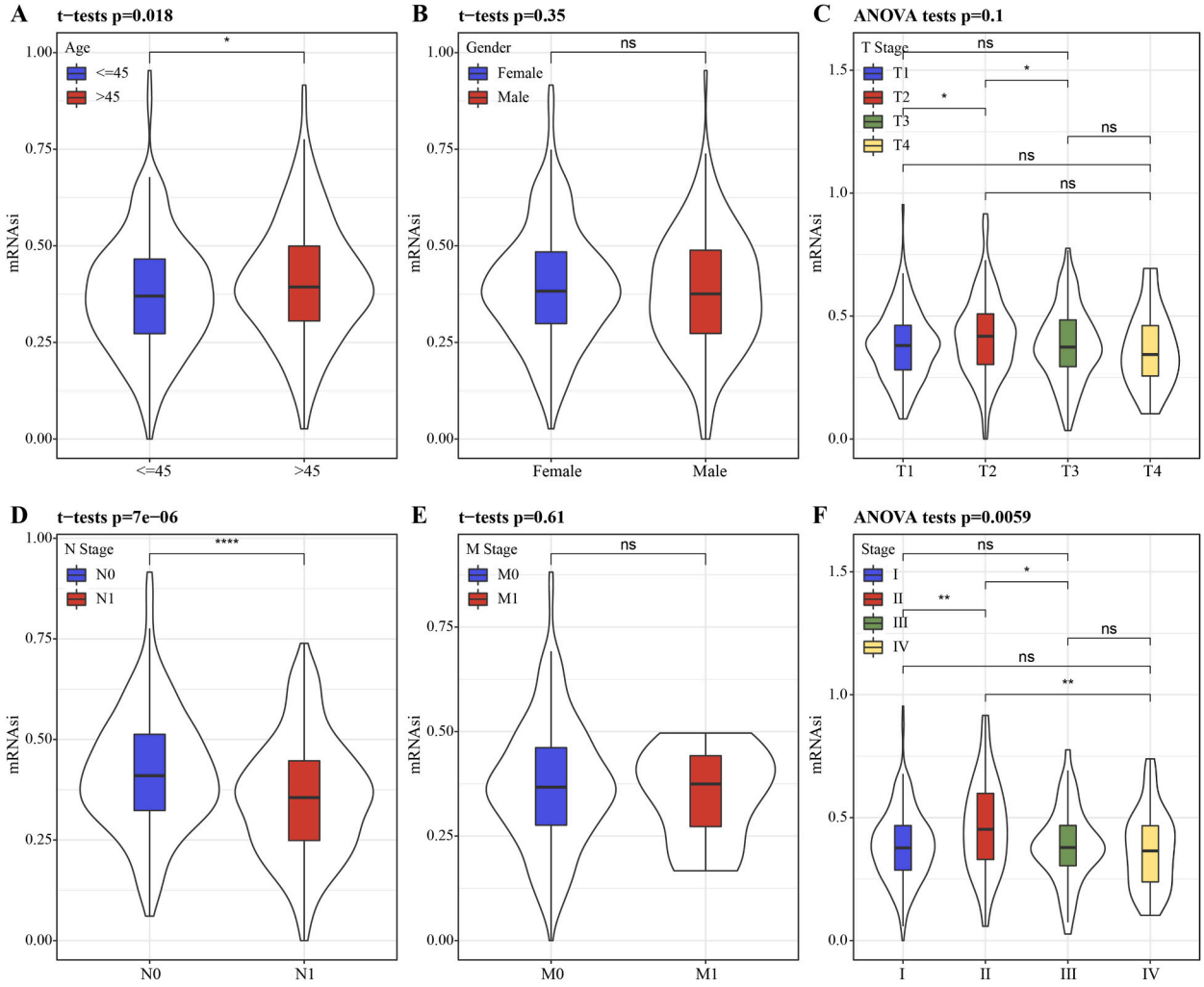

Fig. 3. Relationship between stem cell index and clinical characteristics. A: difference in mRNAsi between samples of different ages; B: difference in mRNAsi between samples of different genders; C: difference in mRNAsi between samples of different T Stages; D: difference in mRNAsi between samples of different N Stages; E: difference in mRNAsi between samples of different M Stage mutations; F: difference in mRNAsi between different Stage mutation samples. *P < 0.05; **P < 0.01; ***P < 0.001; ****P < 0.0001. ns: not significant.

mutations, respectively. The results showed a total of 13 genes were significantly different between the two groups ($P < 0.05$), namely BRAF, CAND1, CELSR1, DNAH9, DNASE2, DOCK7, NRAS, TEX14, TG, UGGT2, UTRN, VPS138, and ZFHX3 (Fig. 2B).

3.2. Correlation between clinical characteristics, stem cell index and the prognosis of THCA

In order to compare whether mRNAsi index differed among different clinical characteristics subgroups of THCA, we compared whether mRNAsi differed among age, gender, T-stage, N-stage, M-stage, and pathological stage subgroups, respectively, and found statistically significant differences in mRNAsi ($P = 0.018$, <0.001, Fig. 3A and D) between tumor samples in the age group ($\leq$45 years, >45 years) and N stage (N0, N1) clinical characteristic group, while the differences in mRNAsi between tumor samples in the gender, T stage, M stage, and pathological stage groups clinical characteristics group were not statistically significant ($P > 0.05$, Fig. 3B–C, 3E-F).

To evaluate whether the mRNAsi was correlated with survival of THCA patients, we first obtained the cut-off values of optimal miRNAsi at different time states using the "survminer" package, then grouped them and plotted the survival K-M curves. Between the high and low mRNAsi groups, the overall survival difference was significant for progression-free interval (PFI) time and disease-free interval (DFI) time (Fig. S1C), while the two subgroups did not show significant differences in disease-specific survival (DSS) and overall survival (OS) (Figs. S1A and D).

3.3. Stem cell index and immune and stromal score analysis

The tumor microenvironment (TME) is constantly evolving [30,37]. We first assessed immune cell infiltration using the "ESTIMATE" algorithm, and then calculated Pearson correlations between immune and stromal scores and mRNAsi, showing that StromalScore ($R = -0.406$, $P < 0.05$), ImmuneScore ($R = -0.142$, $P < 0.05$), EstimateScore ($R = -0.308$, $P < 0.05$) were significantly negatively correlated with the mRNAsi (Fig. 4A–C). Next, we evaluated the scores of 28 immune cells using the "ssGSEA" method and then calculated their correlation with mRNAsi, and found that they also showed a significant negative correlation with mRNAsi (Fig. S2). The correlation between stem cell index and cancer driver genes revealed these 116 cancer driver genes were significantly correlated with mRNAsi (Table S1).

Additionally, we analyzed the mRNAsi and the correlation between mRNAsi and immune scores, found that there was a negative correlation between mRNAsi and StromalScore ($R = -0.73$, $P = 0.000587$) and EstimateScore ($R = -0.496$, $P = 0.0364$) (Fig. S3). Significant negative correlation between 28 immune cells and mRNAsi was observed (Fig. S4).

3.4. Molecular subtyping based on mRNAsi-associated genes

According to the set screening criteria ($|R| > 0.4$, $P < 0.05$), we obtained a total of 1724 genes significantly associated with mRNAsi. Enrichment analysis showed that these genes were associated with TNF signaling pathway, Pathways in cancer, Cytokine-cytokine receptor interaction, TGF-beta signaling pathway, NF-kappa B signaling pathway, MAPK signaling pathway, PI3K-Akt signaling pathway, and other pathways (Fig. S5A). The results showed that mRNAsi-related genes in GSE3467 were closely related to TGF-beta signaling pathway, TNF signaling pathway, and angiogenesis (Fig. S5B).

A total of 37 prognostically significant genes ($P < 0.05$, Fig. 5A), including the Protective genes ADAMT36, CEL8R3, DNM1 ($HR > 1$) and Risk genes SLC17A7, were screened by performing univariate Cox regression analysis. Fig. 5B displays the associations among the 37 genes. The ideal number of clusters according to the CDF was then computed using these 37 differential genes for consistent grouping. The results were obtained by choosing $K = 3$, i.e., three molecular subtypes were classified (Fig. 5C–E). Then, we analyzed the prognostic relationships of the subtypes in the four time points, and found that the subtypes had significant prognostic differences

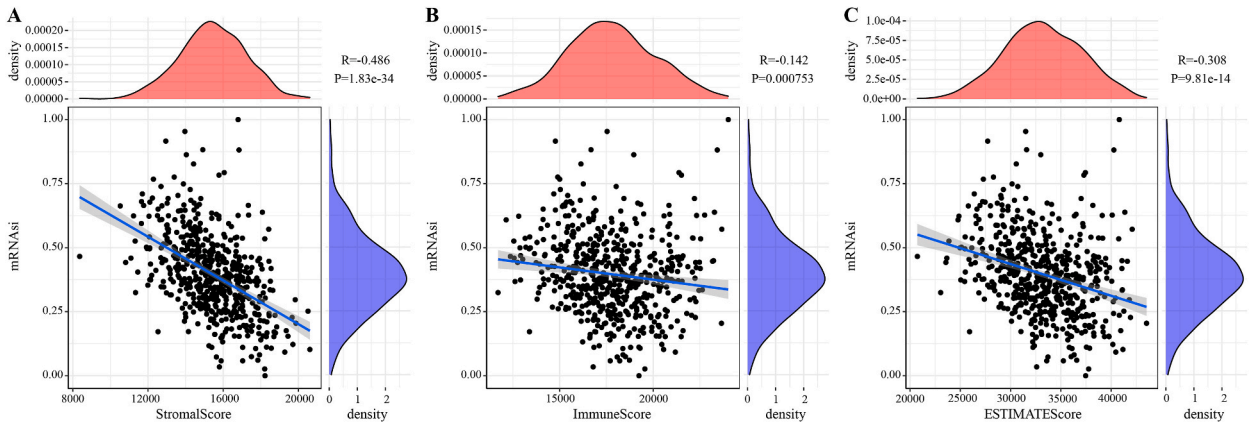

Fig. 4. Immunological characteristics between molecular subtyping based on stem cell index. A: Correlation of sample mRNAsi index with StromalScore in TCGA; B: Correlation of sample mRNAsi index with ImmuneScore in TCGA; C: Correlation of sample mRNAsi index with ESTIMATEScore in TCGA. *$P < 0.05$; **$P < 0.01$; ***$P < 0.001$; ****$P < 0.0001$. ns: not significant.

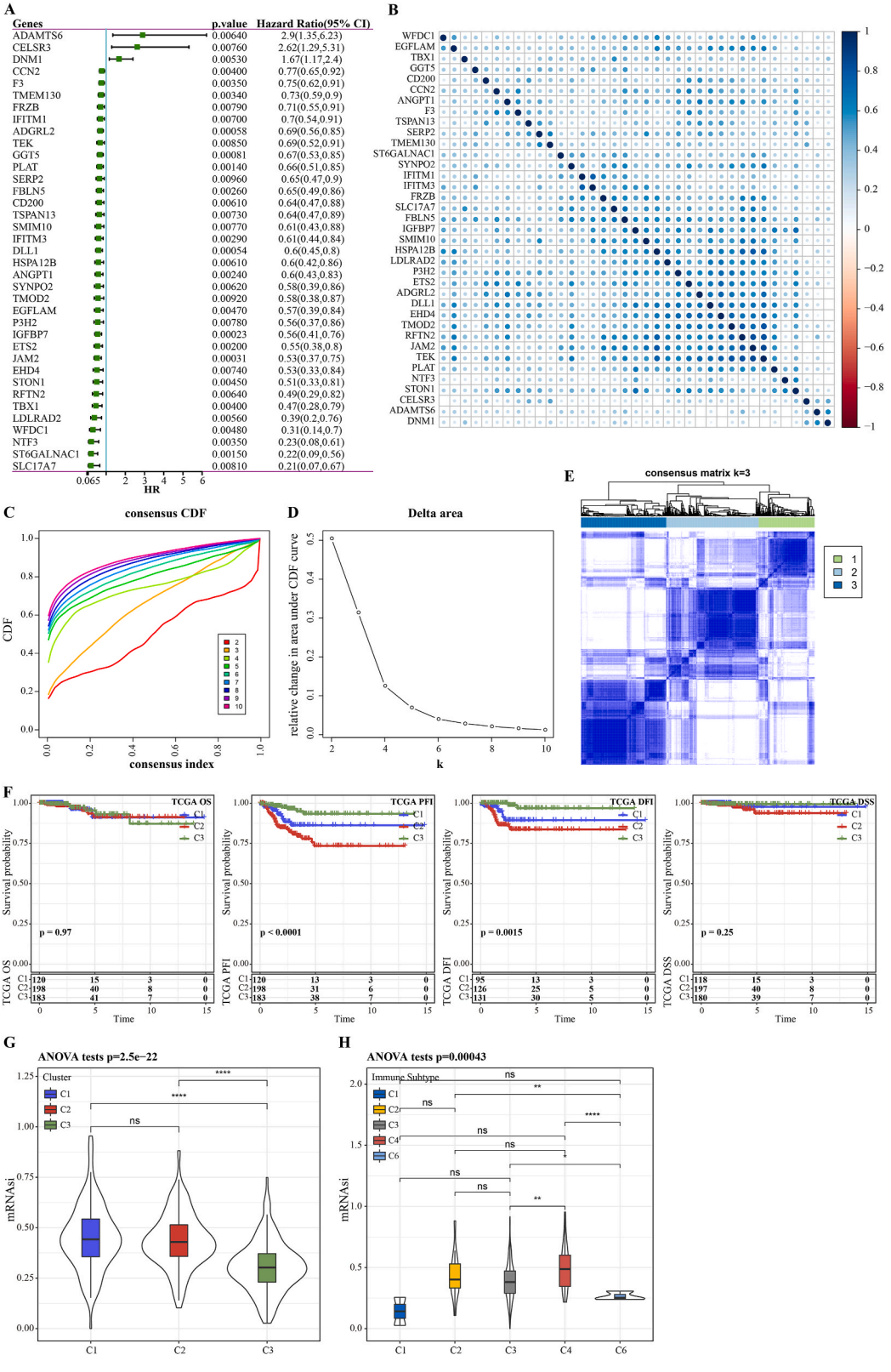

(caption on next page)

Fig. 5. Molecular subtyping based on mRNAsi-related genes A: univariate COX result; B: Correlation analysis of related genes; C–D: CDF curves of TCGA cohort samples and CDF Delta area curves, Delta area curves of consensus clusters, indicating the cumulative compared to k-1 for each category number k distribution function (CDF) curve under the relative change in area. The vertical axis and the horizontal axis indicated the relative change in area under the CDF curve and category number k, respectively; E. Heat map of sample clustering at consensus k = 3; F: prognostic KM curves for TCGA data set subtypes; G: distribution of mRNAsi's among TCGA subtypes; H. distribution of mRNAsi's among existing immune subtypes. *P < 0.05; **P < 0.01; ***P < 0.001; ****P < 0.0001. ns: not significant.

in PFI and DFI (P < 0.05), while the prognostic differences in OS and DSS were not significant (P > 0.05, Fig. 5F). The mRNAsi of the three molecular subtypes demonstrated significant difference (P < 0.05, Fig. 5G). Finally, we obtained the six existing immune subtypes and also compared the differences in the distribution of mRNAsi among the six immune subtypes and found significant differences (P < 0.05, Fig. 5H).

3.5. Clinical and mutation features among THCA molecular subtypes

In the TCGA-THCA cohort, we further investigated the variations in clinicopathological traits among the three distinct molecular subtypes. The differences in PFI status (Fig. S6A), age (Fig. S6B), T-stage (Fig. S6D), N-stage (Fig. S6E), and pathological stage (Fig. S6G) were observed to be statistically significant (P < 0.05) among the three molecular subtypes, whereas there were no significant differences in sex (Fig. S6C) or M-stage(Fig. S6F) with P values > 0.05. The six available immunological subtypes did not significantly differ from one another in terms of the clinical traits (P > 0.05, Fig. S6H). We compared mutant genes between the C1, C2, and C3 subtypes of THCA samples in order to investigate the specific variations in mutant gene expression among the various molecular subtypes. The results revealed that the three most mutant genes among C1, C2, and C3 were BRAF, NRAS, and HRAS (Fig. 6A). Moreover, the distribution of Number of Segments and tumor mutation burden, Fraction Altered among subtypes was compared, and these features differed among subtypes (Fig. 6B).

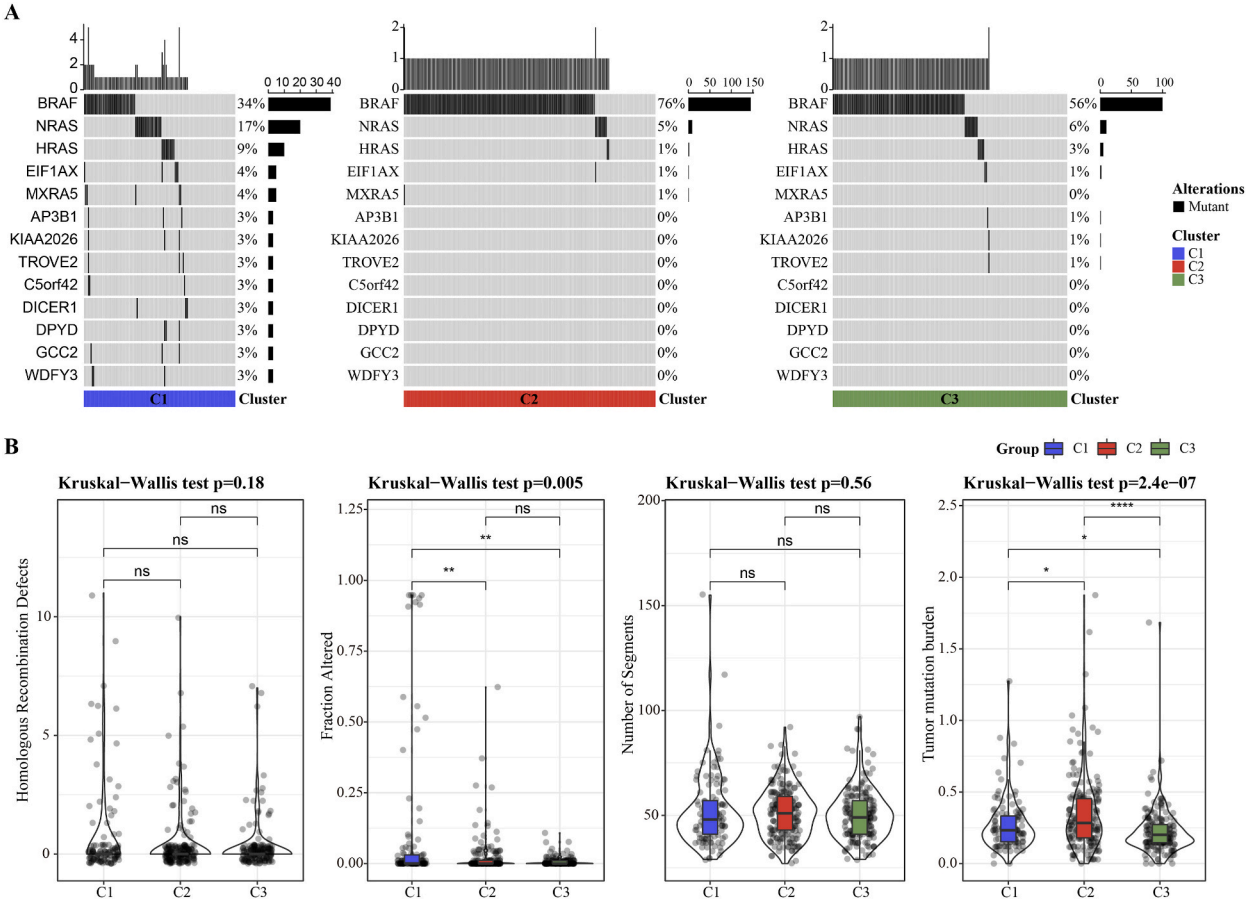

Fig. 6. Mutation characteristics among molecular subtypes. A: Different molecular subtypes in the TCGA cohort (Fisher's exact test) were subjected to somatic mutation analysis; B: Comparison of Homologous Recombination Defects, Tumor mutation burden, Fraction Altered, Number of Segments among different molecular subtypes in the TCGA cohort. *P < 0.05; **P < 0.01; ***P < 0.001; ****P < 0.0001. ns: not significant.

3.6. Prediction of immune characteristics and drug sensitivity among THCA molecular subtypes

We first assessed immune cell infiltration using the "ESTIMATE" algorithm, which showed the highest ImmuneScore, StromalScore, and ESTIMATEScore in the C2 subtype (Fig. S7A). The ssGSEA showed the highest immune score in the C2 subtype (Fig. S7B). This indicated that patients with the C2 subtype may benefit from therapeutic strategies that enhance the immune response. Moreover, the C2 subtype also had the greatest degree of immune checkpoint gene expression (Fig. S7C).

We then evaluated the predictive ability of various molecular subtypes in immunotherapy for cancer, and found significantly higher TIDE score of C3 than C1 and C2, indicating that the two subtypes could benefit more from taking immunotherapy. The predicted analysis of whether an immunotherapy response occurred was 35 % and 38 % in C1 and C2, respectively, which was higher than that in C3 (Fig. 7A). The above results indicated that mRNAsi-based prediction of immunotherapy for THCA was a practical approach. In addition, drug sensitivity prediction found that in the TCGA-THCA cohort, Cisplatin, Erlotinib, Paclitaxel, and Lapatinib drugs were more sensitive in subtype C2, and AKT inhibitor VIII, Sorafenib, Imatinib, and Crizotinib drugs were not sensitive in subtype C2 (Fig. 7B and C).

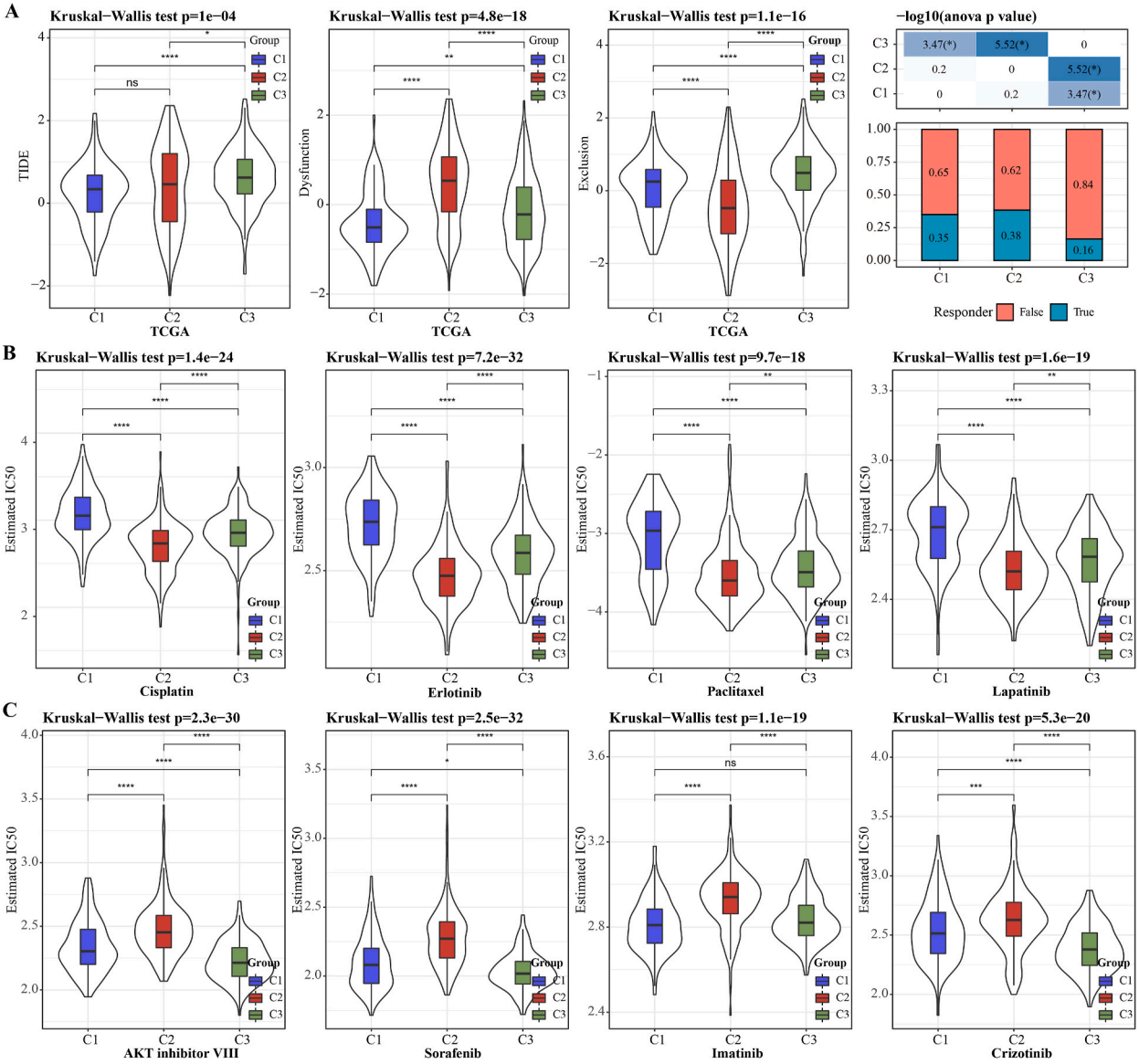

Fig. 7. TIDE of different subtypes and drug sensitivity analysis. A: Differential analysis of TIDE results of different immune subtypes of TCGA; B–C: Differential analysis of drug IC50 of TCGA subtypes. *P < 0.05; **P < 0.01; ***P < 0.001; ****P < 0.0001. ns: not significant.

3.7. Prognostic modeling of THCA

According to the ratio of 1:1, the mRNAsi-related genes in the TCGA-THCA cohort were randomly grouped into Train and Test sets. The differential genes were then subjected to univariate Cox regression analysis, which revealed a total of 9 genes (ADGRL2, CCN2, CELSR3, DNM1, F3, KMT5C, NTF3, STARD9, TMEM130) with a significant prognostic influence. Additionally, we used Lasso analysis to observe the trajectory of each gene, and the model was at its best when lambda = 0.01327193 and related to 6 differential genes (Fig. 8A). Then, using the stepAIC technique in the MASS package, we finally decreased the number of genes to 5, which were CELSR3, F3, NTF3, STARD9, and TMEM130 (Fig. 8B).

Then, we calculated the Riskscore score of each TCGA-THCA patient using these 5 genes and the prognostic model formula (RiskScore = 1.592*CELSR3-0.485*F3-1.329*NTF3+0.707*STARD9-0.437*TMEM130), and classified those with RiskScore>0 as high-risk group, and those with 0≤ were classified as low-risk group based on standardized Zscore value. Next KM curves were plotted for high and low groups (Fig. 8C). In comparison to the low RiskScore grouping, the prognosis for the high RiskScore subgroup was also

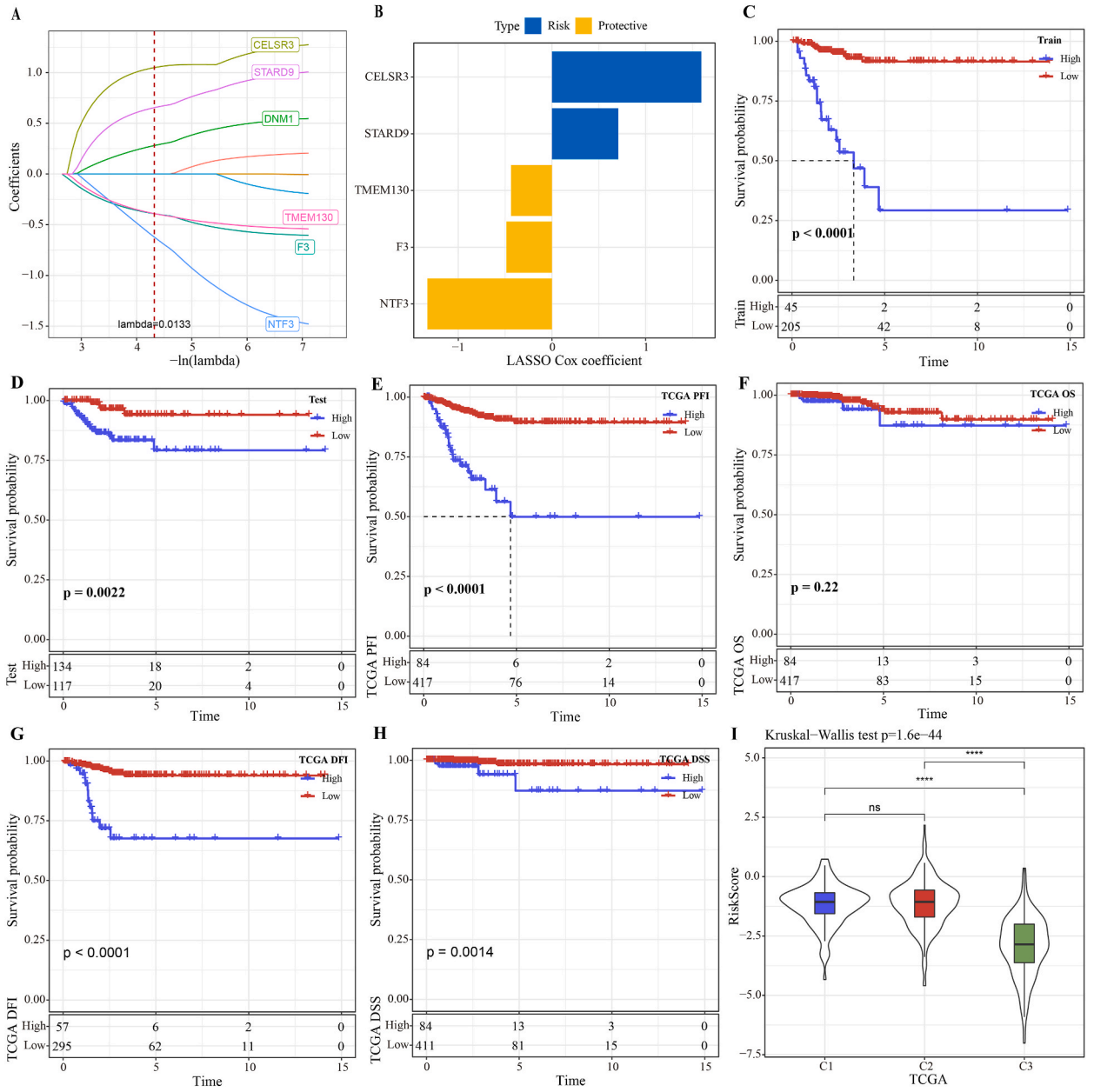

Fig. 8. Construction of prognostic model prediction based on stem cell index. A–F: KM curves of TCGA dataset; G: distribution of RiskScore in subtypes of TCGA dataset. *P < 0.05; **P < 0.01; ***P < 0.001; ****P < 0.0001. ns: not significant.

considerably worse in Test dataset of TCGA (P = 0.001, Fig. 8D). Using PFI, OS, DFI, and DSS as indicators, we also compared the prognosis of the high RiskScore group with that of the low high RiskScore group in total TCGA dataset. Compared to the low RiskScore group, high RiskScore group had a significantly more unfavorable prognosis (Fig. 8E–H). Additionally, we evaluated the variations in the distribution of RiskScore among subtypes in various datasets and discovered that the C3 subgroup had the lowest RiskScore scores,

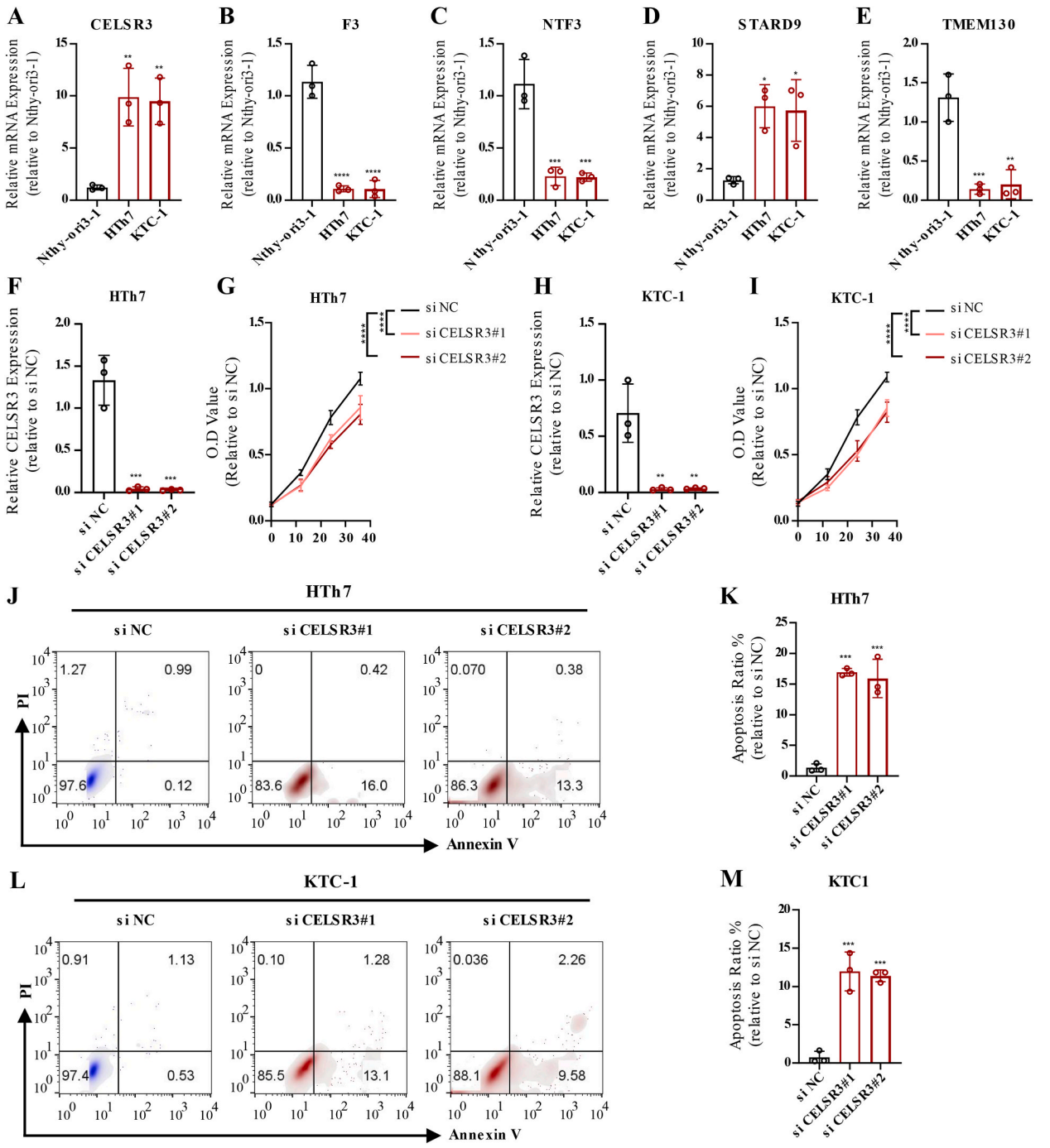

Fig. 9. Experimental validation of bioinformatics model reliability. A–E: Expression of CELSR3, F3, NTF3, STARD9, and TMEM130 detected by qRT-PCR in Hth7, KTC-1, and Nthy-ori3-1. F–G: The inhibition efficiency of small interfering RNA in HTh7 cell lines and the altered viability of Hth7 cell lines after inhibition of CELSR3 expression. H–I: The inhibition efficiency of small interfering RNA in KTC-1 cell lines and the altered viability of KTC-1 cell lines after inhibition of CELSR3 expression. J–K: The alteration of apoptotic ratio in Hth7 cell line after inhibition of CELSR3. L–M: The alteration of apoptotic ratio in KTC-1 cell line after inhibition of CELSR3 expression in HTh7 cell line. N = 3. *≤0.05, **≤0.01, ***≤0.001, ****≤0.0001. N = 3, The results are presented as mean ± SD.

while the C1 and C2 subgroups had the highest RiskScore scores (Fig. 8I).

3.8. Experimental validation of bioinformatics model reliability

The qRT-PCR results showed significantly up-regulated expression of CELSR3 and STARD9 in the thyroid cancer cell lines and suppressed expression of F3, NTF3 and TMEM130 (Fig. 9A–E). This was consistent with the prognostic model predictions revealed in this study. Subsequently, we inhibited the expression of CELSR3 in Hth7 and KTC-1 cell lines (Fig. 9F–H). CCK8 experiments demonstrated that the viability of thyroid cancer cell lines was decreased after the inhibition of CELSR3 expression (Fig. 9G–I). Finally, we examined changes in apoptosis levels after inhibition of CELSR3 expression using flow cytometry. We found that CELSR3 inhibition increased the apoptosis of Hth7 and KTC-1 cells (Fig. 9J-M). The above results invariably illustrate the accuracy of the THCA model used to evaluate patients' prognosis.

3.9. DNA methylation disorder in promoter region of key genes between risk groups

Here we analyzed the methylation profiles of the promoter regions of five key genes, and observed that there are obviously different methylation patterns in high-risk and low-risk patients (Fig. S8A), which suggests that the abnormal expression of these key genes may be related to the methylation imbalance of their promoter regions, Furthermore, we screened the methylation sites significantly related to mRNAsi from the genome. These sites are considered to be the methylation spectrum closely related to tumor stem cells. Through functional enrichment analysis, we can observe that these methylation sites are significantly enriched in Proteoglycans in cancer, Pathways in cancer and other pathways, as well as in regulation of cell morphogenesis, cell − subtract induction and other biological pathways (Fig. S8B). These results indicated that DNA methylation disorder could be an important factor for tumor stem cells to participate in disease progression.

3.10. Performance of the prognostic model RiskScore in pan-cancer

The clinical information and expression profiles of 31 types of solid tumors from the TCGA database were obtained to further test the model performance in pan-cancer. Then we used our RiskScore model to calculate the RiskScore of each cancer type separately and obtain the best cutoff, and performed survival curve analysis for high and low RiskScore. The results showed that except for PCPG ($P = 0.11$), SKCM ($P = 0.12$), and UCS ($P = 0.12$), the RiskScore (high and low) differed significantly in all cancer types, with high RiskScore patients showing a significantly worse prognostic outcome than those with low RiskScore ($P < 0.05$, Fig. S9).

3.11. Comparison of the performance of the prognostic model RiskScore in the immunotherapy dataset

The datasets IMvigor210, GSE91061 was immunotherapy-treated data, in which we calculated RiskScore using our method and used the website TIDE (http://tide.dfci.harvard.edu/) for the assessing the immunotherapy effect TIDE scores, and then compared the predictive effect of RiskScore with TIDE on treatment response. RiskScore and TIDE score were used for curves to predict survival and KM curves with median cutoff. In IMvigor210, patients with high Riskscore survived significantly better than those with low RiskScore

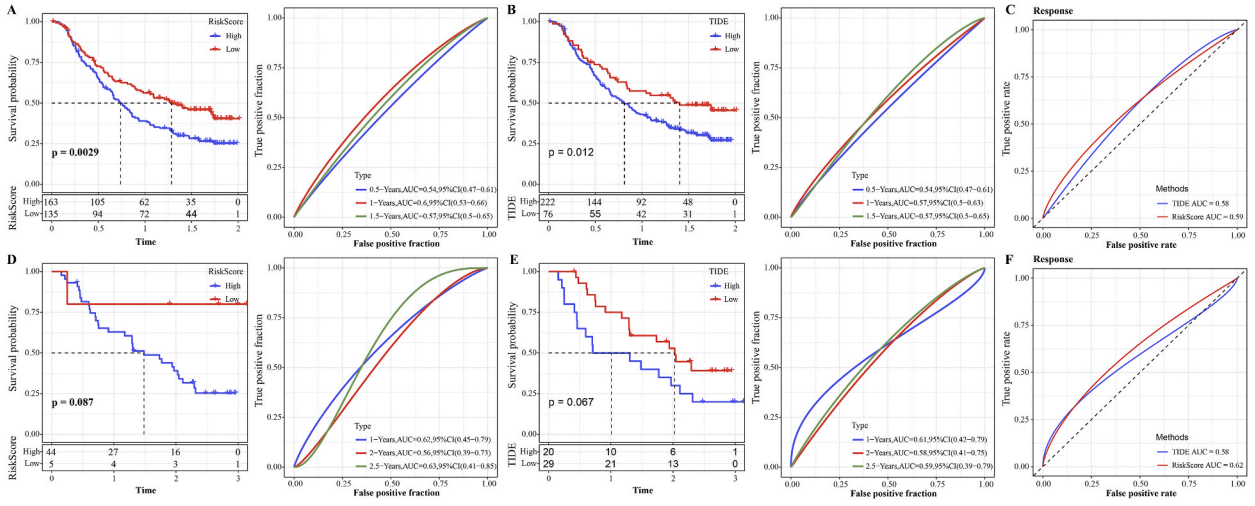

Fig. 10. Comparison of prognostic model performance in immunotherapy dataset. In dataset IMvigor210: A: RiskScore survival curves and ROC curves. B: TIDE survival and ROC curves; C: ROC curves for RISKSCORE and TIDE effects on immunotherapy; In dataset GSE91061: D: RISKSCORE survival and ROC curves; E: TIDE survival and ROC curves; F: ROC curves of the effect of RISKSCORE and TIDE on immunotherapy. *P < 0.05; **P < 0.01; ***P < 0.001; ****P < 0.0001. ns: not significant.

(P = 0.0029), and the area under curve [38] for the predicted probability of survival at 0.5, 1, and 1.5 years was 0.54, 0.6, and 0.57, respectively (Fig. 10A). Next, we grouped THCA patients with TIDE and found that patients with low TIDE scores survived significantly better (P = 0.012), with predicted probability of survival AUCs of 0.54, 0.57, and 0.57 at 0.5, 1, and 1.5 years, respectively (Fig. 10B). Then we compared the Riskscore and TIDE and observed that the AUC of RiskScore was slightly higher than that of TIDE (0.59 > 0.58) with no significance difference (Fig. 10C). Similarly, in the GSE91061 dataset, the survival difference between patients with high and low RiskS-core was not significant (p = 0.087), and the predicted probability of survival at 0.5, 1, and 1.5 years AUCs were 0.62, 0.56, and 0.63, respectively (Fig. 10D). Next, we similarly grouped THCA patients using TIDE and found no significant difference in survival between patients with high and low TIDE score (P = 0.067), with predicted probability of survival AUCs of 0.61, 0.58, and 0.59 at 0.5, 1, and 1.5 years, respectively (Fig. 10E). Finally, RiskScore with TIDE were compared, and it was observed that the AUC of Riskscore was higher than that of TIDE (0.62 > 0.58) (Fig. 10F), and the above results indicated that the Riskscore seems to have similar predicting effect to TIDE score.

4. Discussion

Heterogeneity is a critical characteristic of THCA and a significant factor in unfavorable prognosis [39]. CSCs, by remaining in different states of differentiation, retain the capacity to develop into various types of tumor cells, thereby adding to the heterogeneity. Therefore, subgroup-based classification of CSCs and identification of their biomarkers may become a new and promising approach and provide clues for future treatments.

The generation of thyroid spheres in vitro and the establishment of an in vivo mouse thyroid tumor model both confirmed the presence of THCA stem cells [40,41]. It was shown that the in vitro culture model in the presence of CSC produced large and irregular thyroid spheroids with high clonal potential and high expression levels of stemness markers ABCG2, Oct-4, Sox-2, and EMT markers. Only in the solid tissues of thyroid cancer, stemness spheroids were found to contain Sox-2, Oct-4, CD44, CD133, and Nanog markers [42]. A recent study has revealed that higher level of DAPK1 is related to advanced-stage papillary THCA, with a higher stemness index indicating less favorable DFS [43]. It has been reported that NGF, FOS, and GRIA1 act as novel biomarkers that are closely related to the characteristics of THCA stem cells and have potential for prognosis of THCA patients [44]. However, it is unclear how CSC contributes to the development of THCA and whether the presence of CSC leads to genetic alterations in THCA. To supplement the potential pathogenic mechanism of CSCs on THCA, present study calculated the mRNAsi of each sample and identified five genes as stem cell-associated biomarkers for the pathogenesis of THCA. We also found that CSC may affect the MAPK signaling pathway, Cytokine-cytokine receptor interaction, TGF-beta signaling pathway, NF signaling pathway, NF-kappa B signaling pathway, PI3K-Akt signaling pathway, and other pathways, which suggested that these important pathways in turn contributed to the progression of THCA. Our results provided a new perspective to study the regulatory mechanisms of THCA. In addition, our data showed significant differences in mRNAsi between mutated and non-mutated THCA samples, offering preliminary confirmation that CSC may lead to alterations in the genetic landscape of THCA.

The first obstacle to tumorigenesis is immune surveillance. CSC represents a heterogeneous subpopulation of cells capable of modulating the host immune response and evading immune cell-mediated attack. During the escape phase, CSCs are in a quiescent and low-immunogenic state, which facilitates non-recognition of tumor by the host immune system [45]. Immune cells with pro- and anti-tumor effects, including tumor-associated macrophages, neutrophils and basophils, are present in the thyroid tumor microenvironment [46]. A study has deciphered that less immune infiltration and a large number of CSCs in the TME contribute to the dismal prognosis of papillary THCA [47]. Unfortunately, few studies analyze the differences of immune characteristics in THCA with different molecular subtypes. Consistent with existing studies [48,49]. The current findings demonstrated significant difference in immune cell scores and stromal cell scores in THCA with different molecular subtyping, implying that CSC influenced the immune cell composition of THCA, which shed new insights into the role of CSC in immune characteristics. Furthermore, we performed an analysis of specific types of immune cells, and the results similarly confirmed that the C2 subtype had the highest immune scores. In addition, basal experiments showed that immune cell-derived cytokines have a key role in THCA generation, survival, proliferation and resistance, leading to increased expression of stemness markers Oct-4 and CD133 [50]. Our study confirmed that CSC and stromal cells can interact with each other to promote tumor metastasis by recruiting immune cell cells or influencing cytokine expression, thus supporting THCA progression.

Hypofractionated and undifferentiated THCA are poorly treated with conventional therapy due to their malignant behavior such as recurrence and invasive metastasis, with an overall median survival of only 2–6 months [51]. Chemotherapy drug resistance is a major challenge in the treatment of malignant THCA, and chemoresistance, recurrence and metastasis, which contribute to the poor prognosis of THCA, and are all associated with CSC [52]. Wang and colleagues have demonstrated that MAPK12 is closely associated with the immune checkpoint, microsatellite instability, and affected the immunotherapy sensitivity [53]. However, there is lacking molecular subtypes for THCA classification and chemotherapy/immunotherapy. Here, we classified patients into three subtypes based on mRNAsi, which provided supplements for clinical classification for THCA patients. We also found that in the TCGA-THCA cohort, Cisplatin, Erlotinib, Paclitaxel, and Lapatinib were more sensitive in the C2 subtype, while AKT inhibitor VIII, Sorafenib, Imatinib, and Crizotinib drugs were not sensitive in subtype C2. The above results implied that mRNAsi-based prediction of immunotherapy and chemotherapy for THCA was a practical approach to maximize THCA patients' survival and helped realize the goal of precision medicine.

Developing risk models to screen high-risk groups of THCA is a more accurate approach. The current study successfully constructed prediction models by determining the expression levels and expression coefficients of CELSR3, F3, NTF3, STARD9, TMEM130 and divided patients into two groups with high and low risk. Among them, CELSR3 belongs to the calmodulin superfamily, and the encoded

protein may be involved in regulating the growth of contact-dependent neuroprotrusions and may play a role in tumor formation. Studies have shown that CELSR3 protein is often high-expressed in tumor tissues, and its downregulation significantly inhibits the proliferation and migratory potential of tumor cells. F3 encodes coagulation factor III, which allows the initiation of coagulation cascade and cells to function as a high-affinity receptor for coagulation factor VII [54]. As a member of the neurotrophin family, NTF3, which could be used to control mammalian neurons survival and differentiation, is closely related to nerve growth factors and brain-derived neurotrophic factors. Animal experiments have shown that NTF3 activates TrkB to induce apoptotic resistance in tumor cell loss, suggesting that NTF3 is also a direct target for anticancer [55]. STARD9 is a recently identified centrosomal protein, it has been found to be able to regulate the stability and assembly of spindle microtubules and interphase microtubules, thus playing an important role in tumor cell cycle progression [56]. In addition, there are also studies suggest that TMEM130 downregulation and hypermethylation may contribute to breast cancer cell metastasis, and thus TMEM130 may be a promising tumor biomarker [57]. Remarkably, there is a gap in research on the molecular mechanisms of F3 development in cancer. In contrast, in the present study, we revealed for the first time the potential role of F3 in THCA, whose expression is down-regulated in cancer cells. These results further reveal that the prognostic genes we identified based on CSC characteristics may have a potential impact on THCA patients and provide new insights and directions for the treatment of THCA.

Nevertheless, there are limitations in this study. Although we have validated the risk model in this study, the molecular mechanism of cancer regulation by model signature genes requires more specific cellular experiments, and experiments such as CCK-8 and flow cytometry carried out in the preliminary stage of this study are not sufficient to reveal this molecular mechanism. Retrospective data was obtained from the public database which might induce bias. Thus, more prospective researches with large sample size should be carried out to verify the results. Besides, the role of post translation modifications such as protein modification should be investigated in the future. Finally, drug sensitivity analyses lack the support of more in-depth clinical data. For this reason, further studies will be based on in vivo and in vitro experiments to investigate the expression and functional status of these drug targets of action in different subtypes.

5. Conclusions

This study performed subtyping based on patients in the TCGA-THCA cohort by calculating the stem cell index mRNAsi and found significant differences in clinical features, mutated genes, and immune composition among subtypes. A prognostic model was established using genes related to mRNAsi, with a strong robustness and favorable results in predicting immunotherapy response as well as in pan-cancer.

Ethical statement

Informed consent was not required for this study because it is not involved any human experiments.

Funding

The author(s) received no specific funding for this work.

Data availability statement

The datasets are available at GEO: GSE3467 [https://www.ncbi.nlm.nih.gov/geo/query/acc.cgi?acc=GSE3467], GSE91061 [https://www.ncbi.nlm.nih.gov/geo/query/acc.cgi?acc=GSE91061].

CRediT authorship contribution statement

Ruoran Chen: Writing – review & editing, Writing – original draft, Software, Resources, Formal analysis, Conceptualization. **Wei Gao:** Writing – original draft, Validation, Software, Resources, Methodology, Data curation. **Linlang Liang:** Visualization, Resources, Investigation, Data curation. **Hao Yu:** Visualization, Validation, Project administration, Investigation. **Wei Song:** Resources, Project administration, Methodology, Data curation.

Declaration of competing interest

The authors declare that they have no known competing financial interests or personal relationships that could have appeared to influence the work reported in this paper.

Acknowledgement

None.

Appendix A. Supplementary data

Supplementary data to this article can be found online at https://doi.org/10.1016/j.heliyon.2024.e31970.

Abbreviations

mRNAsi	mRNA expression-based stemness index
THCA	thyroid cancer
TCGA	Tumor Genome Atlas Project
PCBC	Progenitor Cell Biology Consortium
OCLR	class logistic regression
CSC	cancer stem cells
ssGSEA	Single Sample Gene Set Enrichment Analysis
PCG	protein coding gene
CDF	cumulative distribution function
AIC	Akaike information criterion
PFI	progression-free interval
DFI	disease-free interval
DSS	disease-specific survival
TME	The tumor microenvironment

References

[1] D.W. Chen, et al., Thyroid cancer, Lancet 401 (10387) (2023) 1531–1544.
[2] U. Khan, et al., Patient and tumor factors contributing to distant metastasis in well-differentiated thyroid cancer: a retrospective cohort study, J. Otolaryngol. Head Neck Surg. 49 (1) (2020) 78.
[3] Q. Xiaoyu, et al., Development and validation of a novel defined 7-methylguanosine-related gene signature to prognose thyroid cancer outcomes, J. Biol. Regul. Homeost. Agents 37 (2) (2023) 1029–1039.
[4] F. Cappellacci, et al., Technological innovations in thyroid cancer surgery, Oncologie 24 (1) (2022) 35–50.
[5] K.A. Araque, S. Gubbi, J. Klubo-Gwiezdzinska, Updates on the management of thyroid cancer, Horm. Metab. Res. 52 (8) (2020) 562–577.
[6] A.J. Bauer, Pediatric thyroid cancer: genetics, therapeutics and outcome, Endocrinol Metab. Clin. N. Am. 49 (4) (2020) 589–611.
[7] S.N. Silva, Special issue: genetic perspectives in thyroid cancer, Genes 12 (2) (2021).
[8] Y. Xiao, et al., A nomogram for predicting lateral lymph node metastasis in cases of papillary thyroid micro-carcinoma with suspected lymph node metastasis, Oncologie 23 (2) (2021) 219–228.
[9] D. Bonnet, J.E. Dick, Human acute myeloid leukemia is organized as a hierarchy that originates from a primitive hematopoietic cell, Nat. Med. 3 (7) (1997) 730–737.
[10] W. Yin, et al., Cancer and stem cells, Exp. Biol. Med. 246 (16) (2021) 1791–1801.
[11] Y. Matsushita, W. Ono, N. Ono, Synergy of single-cell sequencing analyses and in vivo lineage-tracing approaches: a new opportunity for stem cell biology, Biocell 46 (5) (2022) 1157–1162.
[12] D.-K.-W. Ocansey, et al., Mesenchymal stem cell-derived exosome: the likely game-changer in stem cell research, Biocell 46 (5) (2022) 1169–1172.
[13] L. Yang, et al., Targeting cancer stem cell pathways for cancer therapy, Signal Transduct. Targeted Ther. 5 (1) (2020) 8.
[14] Q. Liu, et al., Identification of cancer stem cells derived from U118MG and the involvement of LncRNA-DC and STAT3 in promoting their malignant transformation, Oncologie 25 (2) (2023) 199–209.
[15] X.W. Pan, et al., Identification of a novel cancer stem cell subpopulation that promotes progression of human fatal renal cell carcinoma by single-cell RNA-seq analysis, Int. J. Biol. Sci. 16 (16) (2020) 3149–3162.
[16] S. Karmakar, et al., RNA polymerase II-associated factor 1 regulates stem cell features of pancreatic cancer cells, independently of the PAF1 complex, via interactions with PHF5A and DDX3, Gastroenterology 159 (5) (2020) 1898–1915.e6.
[17] H. Lu, et al., Targeting cancer stem cell signature gene SMOC-2 Overcomes chemoresistance and inhibits cell proliferation of endometrial carcinoma, EBioMedicine 40 (2019) 276–289.
[18] A.K. Croker, A.L. Allan, Cancer stem cells: implications for the progression and treatment of metastatic disease, J. Cell Mol. Med. 12 (2) (2008) 374–390.
[19] A. Fierabracci, et al., Identification of an adult stem/progenitor cell-like population in the human thyroid, J. Endocrinol. 198 (3) (2008) 471–487.
[20] P. Zhang, et al., Cancer stem cell hypothesis in thyroid cancer, Pathol. Int. 56 (9) (2006) 485–489.
[21] N. Singh Ospina, N.M. Iñiguez-Ariza, M.R. Castro, Thyroid nodules: diagnostic evaluation based on thyroid cancer risk assessment, BMJ 368 (2020) l6670.
[22] T.M. Malta, et al., Machine learning identifies stemness features associated with oncogenic dedifferentiation, Cell 173 (2) (2018) 338–354.e15.
[23] M. Zhou, X. Sun, Y. Zhu, Analysis of the role of Frizzled 2 in different cancer types, FEBS Open Bio 11 (4) (2021) 1195–1208.
[24] S. Pei, et al., Benchmarking variant callers in next-generation and third-generation sequencing analysis, Briefings Bioinf. 22 (3) (2021).
[25] B. Chen, et al., Profiling tumor infiltrating immune cells with CIBERSORT, Methods Mol. Biol. 1711 (2018) 243–259.
[26] H. Chakraborty, A. Hossain, R package to estimate intracluster correlation coefficient with confidence interval for binary data, Comput. Methods Progr. Biomed. 155 (2018) 85–92.
[27] Y. Jin, et al., Identification of novel subtypes based on ssGSEA in immune-related prognostic signature for tongue squamous cell carcinoma, Cancer Med. 10 (23) (2021) 8693–8707.
[28] J. Gao, et al., Integrative analysis of complex cancer genomics and clinical profiles using the cBioPortal, Sci. Signal. 6 (269) (2013) pl1.
[29] J. Azman, et al., [Correlation and regression], Acta Med. Croat. 60 (Suppl 1) (2006) 81–91.
[30] H. Zhang, et al., The molecular feature of macrophages in tumor immune microenvironment of glioma patients, Comput. Struct. Biotechnol. J. 19 (2021) 4603–4618.
[31] P. Wu, W. Sun, H. Zhang, An immune-related prognostic signature for thyroid carcinoma to predict survival and response to immune checkpoint inhibitors, Cancer Immunol. Immunother. 71 (3) (2022) 747–759.
[32] P. Jiang, et al., Signatures of T cell dysfunction and exclusion predict cancer immunotherapy response, Nat. Med. 24 (10) (2018) 1550–1558.

[33] P. Geeleher, N. Cox, R.S. Huang, pRRophetic: an R package for prediction of clinical chemotherapeutic response from tumor gene expression levels, PLoS One 9 (9) (2014) e107468.
[34] N. Simon, et al., Regularization paths for cox's proportional hazards model via coordinate descent, J. Stat. Software 39 (5) (2011) 1–13.
[35] Y. Tian, et al., ChAMP: updated methylation analysis pipeline for Illumina BeadChips, Bioinformatics 33 (24) (2017) 3982–3984.
[36] Z. Song, et al., CHDTEPDB: transcriptome expression profile database and interactive analysis platform for congenital heart disease, Congenit. Heart Dis. 18 (6) (2023) 693–701.
[37] L. Wu, et al., Seven genes associated with lymphatic metastasis in thyroid cancer that is linked to tumor immune cell infiltration, Front. Oncol. 11 (2021) 756246.
[38] M.K. Tripathi, et al., Nuclear factor of activated T-cell activity is associated with metastatic capacity in colon cancer, Cancer Res. 74 (23) (2014) 6947–6957.
[39] E. Chmielik, et al., Heterogeneity of thyroid cancer, Pathobiology 85 (1–2) (2018) 117–129.
[40] L. Zhang, et al., Diallyl trisulphide, a H(2) S donor, compromises the stem cell phenotype and restores thyroid-specific gene expression in anaplastic thyroid carcinoma cells by targeting AKT-SOX2 axis, Phytother Res. 35 (6) (2021) 3428–3443.
[41] R.Y. Lin, Thyroid cancer stem cells, Nat. Rev. Endocrinol. 7 (10) (2011) 609–616.
[42] V. Carina, et al., Multiple pluripotent stem cell markers in human anaplastic thyroid cancer: the putative upstream role of SOX2, Thyroid 23 (7) (2013) 829–837.
[43] M.H. You, et al., Death-associated protein kinase 1 inhibits progression of thyroid cancer by regulating stem cell markers, Cells 10 (11) (2021).
[44] T. Zhang, et al., The identification of three key genes related to stemness in thyroid carcinoma through comprehensive analysis, Comb. Chem. High Throughput Screen. 24 (3) (2021) 423–432.
[45] D. Bayik, J.D. Lathia, Cancer stem cell-immune cell crosstalk in tumour progression, Nat. Rev. Cancer 21 (8) (2021) 526–536.
[46] M. Peng, et al., Single-cell transcriptomic landscape reveals the differences in cell differentiation and immune microenvironment of papillary thyroid carcinoma between genders, Cell Biosci. 11 (1) (2021) 39.
[47] Z. Xie, YuHe XinLun, SongWang YuzhenWu, JianjianHe ShiyueSun, YuchenXin, ShijieZhangJian, Papillary thyroid carcinoma with a high tumor mutation burden has a poor prognosis, Int. Immunopharm. 89 (Pta2) (2020).
[48] J.A. Clara, et al., Targeting signalling pathways and the immune microenvironment of cancer stem cells - a clinical update, Nat. Rev. Clin. Oncol. 17 (4) (2020) 204–232.
[49] E. Menicali, et al., Immune landscape of thyroid cancers: new insights, Front. Endocrinol. 11 (2020) 637826.
[50] K.T. Bauerle, et al., Nuclear factor κB-dependent regulation of angiogenesis, and metastasis in an in vivo model of thyroid cancer is associated with secreted interleukin-8, J. Clin. Endocrinol. Metab. 99 (8) (2014) E1436–E1444.
[51] T. Ibrahimpasic, et al., Poorly differentiated carcinoma of the thyroid gland: current status and future prospects, Thyroid 29 (3) (2019) 311–321.
[52] H. Wang, et al., Targeting ALDH1A1 to induce necroptosis in nasopharyngeal carcinoma, J. Cancer 13 (14) (2022) 3515–3525.
[53] J. Wang, et al., Pan-cancer analysis supports MAPK12 as a potential prognostic and immunotherapeutic target in multiple tumor types, including in THCA, Oncol. Lett. 24 (6) (2022) 445.
[54] D. Merrick, et al., Identification of a mesenchymal progenitor cell hierarchy in adipose tissue, Science 364 (6438) (2019).
[55] E.N. Howe, et al., miR-200c targets a NF-κB up-regulated TrkB/NTF3 autocrine signaling loop to enhance anoikis sensitivity in triple negative breast cancer, PLoS One 7 (11) (2012) e49987.
[56] S. Srivastava, D. Panda, A centrosomal protein STARD9 promotes microtubule stability and regulates spindle microtubule dynamics, Cell Cycle 17 (16) (2018) 2052–2068.
[57] H. Liu, et al., DNA methylation-mediated down-regulation of TMEM130 promotes cell migration in breast cancer, Acta Histochem. 123 (8) (2021) 151814.